Optimization of Energy Supplies for Floating LiDAR System at Baron Coast, Indonesia using Genetic Algorithms

Didik Rostyono*, Rudi Purwo Wijayanto**, Amiral Aziz*‡, Khotimatul Fauziah*‡, Toha Zaky*, Nurry Widya Hesty*, Ifanda*, Ridwan Budi Prasetyo***, Ario Witjakso*, Agustina Putri Mayasari****

*Research Center for Energy Conversion and Conservation, National Research and Innovation Agency Republic of Indonesia (BRIN), South Tangerang 15314 Indonesia

**Directorate of Technology Transfer and Audit System, National Research and Innovation Agency Republic of Indonesia (BRIN), South Tangerang 15314 Indonesia

***Research Center for Hydrodynamic Technology, National Research and Innovation Agency Republic of Indonesia (BRIN), Yogyakarta 55284 Indonesia

****BKPUK, National Research and Innovation Agency Republic of Indonesia, South Tangerang 15314 Indonesia

(didi007@brin.go.id, rudi014@brin.go.id, amiral.aziz@brin.go.id, khot001@brin.go.id, toha002@brin.go.id, nurr010@brin.go.id, ifanda@brin.go.id, ridw007@brin.go.id, ario001@brin.go.id, agus133@brin.go.id)

‡Corresponding Author; Amiral Aziz, Khotimatul Fauziah, Research Center for Energy Conversion and Conservation, National Research and Innovation Agency Republic of Indonesia (BRIN), South Tangerang 15314 Indonesia,

amiral.aziz@brin.go.id, khotimatul.fauziah@brin.go.id

Received: 18.12.2023 Accepted:26.01.2024

Abstract- The use of renewable energy for commercial and domestic use in Indonesia has grown relatively high in the last decade. Eventually, the development of renewable power plants will intersect with land use for commercial because renewable energy resources are available only in certain locations. In the future, using lakes and seas for renewable power generation locations is an option. However, measuring the potential of wind energy in the ocean is an activity that has yet to be carried out widely. The floating LiDAR system (FLS) is an alternative technology for wind resources measurement at offshore applications. In order to obtain the optimum size of FLS power supplies for the Baron Coast application, it is necessary to optimize the process with the objective function of minimizing energy production costs. In this paper, optimization using a Genetic Algorithm (GA) is carried out to reduce energy costs and unmet load with combinations of renewable energy resources to supply the FLS's load and batteries. The optimization's result will be verified by HOMER software. Based on the simulation result, compared to HOMER, a GA-based combination of 100% PV and 0% backup power is the optimal solution to supply energy with 0% unmet load at the optimum cost of energy of IDR 5,200/kWh.

Keywords Floating LiDAR, offshore, wind measurement, genetic algorithm, energy supply.

1. Introduction

Wind speed measurement is a crucial part of wind resource assessment to estimate the future energy production of a wind power plant. Generally, wind speed measurements are carried out by installing anemometers, wind vanes, and other sensors at certain heights on a meteorological tower according to the wind turbine hub height. In the last decade, wind turbines' size has grown in height and blade length. In 2021, the average hub height of land-based wind turbines will

be around 94 meters [1]. Turbine towers are becoming taller to capture more energy since winds generally increase as altitudes increase. Wind can flow more freely at higher heights, with less friction from obstacles on the earth's surface, such as trees and other vegetation, buildings, and mountains.

The increase in hub height of wind turbines is closely related to wind speed measurement using the conventional meteorological tower. There are more issues with using the taller meteorological mast, such as the cost of the tower, the tower design, permits, installation difficulties, potential lightning strikes, footprint area requirements, accuracy, etc. Furthermore, installing meteorological masts in offshore locations involves highly technical and financial calculations [2–4]. Due to the shortcomings of the meteorological tower mentioned above, alternative technologies that use remote sensing systems, such as Sonic Detection and Ranging (SoDAR) and Light Detection and Ranging (LiDAR), are introduced. LiDAR uses the Doppler effect to precisely measure air movement at higher altitudes. Ground-based measurement devices shoot laser beams into the sky. This beam hits particles and aerosols in the air, a process that reflects light. The duration period of this process can be used to calculate the height. The system can determine the speed and direction of the wind with the help of the Doppler shift, which causes the movement of the back-scattering particles.

Using LiDAR technology to measure wind speed has grown in interest in the wind energy community [5,6]. However, the movement of the sea imparting motion on the LiDAR and the remoteness of the system required a robust and reliable system, including power availability [7]. Applying these two offshore wind measurement technologies is acceptable to both wind developers and banks. The final decision between the two technologies depends on costs. The cost of a 100-meter meteorological tower in the US, for example, falls roughly in the range of $80,000 to $130,000; meanwhile, a shorter, tilt-up 60-meter met mast can be deployed for $25,000–40,000 (excluding permit fees). The equivalent for a 200-meter vertical-profiling LiDAR would be around $175,000 and for an approximately 120-meter vertical-profiling SoDAR, $60,000–70,000. Maintenance costs vary widely, especially if a remote sensing unit has to be returned to the factory for service, although some can be field-maintained. However, offshore installation of these technologies requires different complexity and cost. There are several criteria that have to be considered to determine the location of installation of the offshore wind system: wind speed, water depth and seabed conditions, distance to shore, and distance to the distribution network [8].

Li et al. [9] demonstrated the ZephIR LiDAR system to evaluate wind energy potential at 30 m and 70 m heights at the site near Lake Erie in Ohio, which indicates satisfactory data results compared to the actual wind turbine power output. Gottschall et al. [10] reported a trial of floating LiDAR prototype Fraunhofer IWES Wind Lidar Buoy using a motions correction algorithm and showed a good correlation with the reference of an offshore met mast. Viselli et al. [11] validated the measurement accuracy of the first floating LiDAR buoy DeepCLiDAR in the Northeast US and verified it with land-based reference LiDAR. Moreover, Viselli et al. [12] presented wind speed shear exponents and turbulence intensity (TI) measurements of DeepCLiDAR and compared them against industry guidelines. Gautam et al. [13] studied estimation methods and performance comparison of LiDAR at heights up to 200 m and met mast at heights up to 100 m for wind resource assessment in an Indian offshore location.

A significant weakness of LiDAR compared to meteorological towers is the power consumption. The LiDAR consumes up to 70 watts to emit a laser beam to the sky continuously, excluding other loads; therefore, a certain power or energy supply is needed if it is used in remote areas far from power grids, such as offshore wind speed measurements. The most widely used power sources are combinations of renewable resources, such as solar and wind, and storage devices, like batteries or fuel cells. One of the known causes of floating LiDAR system. Availability issues could be more accurate regarding renewable energy sources' effectiveness [14].

This paper discusses the optimization process to obtain the optimum size and combinations of FLS power supplies for the Baron Coast application with the objective function of minimizing energy-generating costs. A genetic algorithm is a powerful method for finding the optimal solutions in combinatorial and multi-objective optimization problems [15–18]. Therefore, this study proposed a genetic algorithm approach to find an optimal size and combination of renewable energy resources for supplying FLS. The proposed methods are then evaluated in MATLAB. Furthermore, the simulation results are compared to HOMER Pro software to validate the optimization results of the proposed approach.

2. Material and Methods

2.1. Baron Coast Bathymetry

A study on marine and coastal geology at the coast of Yogyakarta was carried out by the Marine Geological Institute in 2002, showing that the characteristics of the beaches in the study area can be divided into two types of beaches. Type 1 beach covers the area along the coast from Sadeng Bay to Parangtritis, characterized by white sand beaches resulting from debris from limestone reefs, karst topographic formations with high relief and cliffs, winding coastlines forming bays and headlands. Meanwhile, the Type 2 beach is located west of the study area. It is characterized by the constituent sediments in blackish-gray sand resulting from debris from volcanic rock products, as presented in Fig. 1.

Sloping morphology with low relief and dunes on the beach characterize the shape of a straight coastline. The slope of the beach is relatively steep, the berm is wide, and the beach is over 200 meters long. The seabed depth measurements show that the Baron coast has a contour pattern parallel to the coastline, which gradually gets deeper towards the open sea, with depth values from the coastline up to 12 miles ranging from 5 meters to 350 meters. Bathymetric analysis in the Gunung Kidul area with an exaggeration profile of 11.4 times and a gradient of 2.5%, as given in Fig. 2, while the analysis with an exaggeration profile of 17.9 times and a gradient of 1.14% is depicted in Fig. 3. Since the depth of the Baron coast

is above 50 meters, the floating type is the most suitable platform to be applied as a remote wind measurement [19].

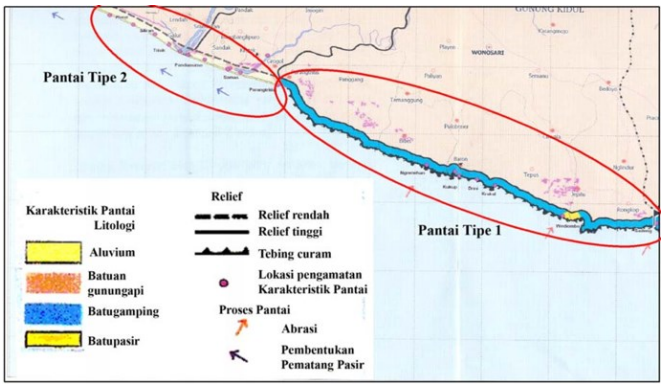


Fig. 1. Seabed map of the South coast of Yogyakarta.



Fig. 2. Map of the seabed of Baron coast.

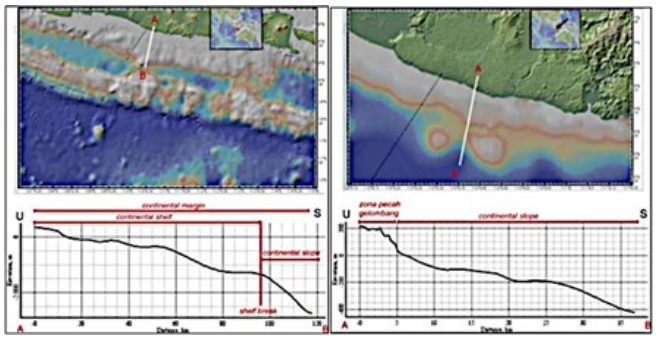


Fig. 3. Bathymetric analysis in the Gunung Kidul area.

2.2. Renewable Energy Potential

Baron has settled in the Gunung Kidul district of Special Province Yogyakarta, approximately 40 kilometers from the capital city. Gunung Kidul has a large wind potential area compared to other areas in Java island, Indonesia with wind speeds above 5,7 m/s, according to the potential wind map from EMD-Indonesia as shown in Fig. 4. Most of the potential area is called "sultan ground," i.e., the customary land where the land is a legacy belonging to the Yogja Palace institution. The state has given special authority to "Daerah Istimewa Yogyakarta" through Law No. 13 of 2012 concerning the Privileges of the Special Region of Yogyakarta. Due to the current landowner status, developing offshore areas for wind turbines or wind farm utilization needs to be considered.

Since 2004, several meteorological towers have been erected by research institutions and wind developers to measure wind potential in the Baron area. The summaries of wind measurements in that area are represented in the wind speed distribution curve, and wind directions are shown in Fig. 5. Meanwhile, the exact number of events for wind speed distribution at 50 m, 35 m, and 20 m heights is shown in Table 1. The measurement of solar radiation at Baron is still ongoing today. The measuring devices are installed on the rooftop of the Baron Techno Park building, and the real-time data can be viewed online through Indonesia Solar Map website, provided by the AESI (the Indonesia solar energy association). Based on the solar power potential map from the Global Solar Atlas, as shown in Fig. 6, the Gunung Kidul area has an irradiation of about 4 kWh/day. The solar radiation data can also be retrieved from the Homer software, as shown in Fig. 7.

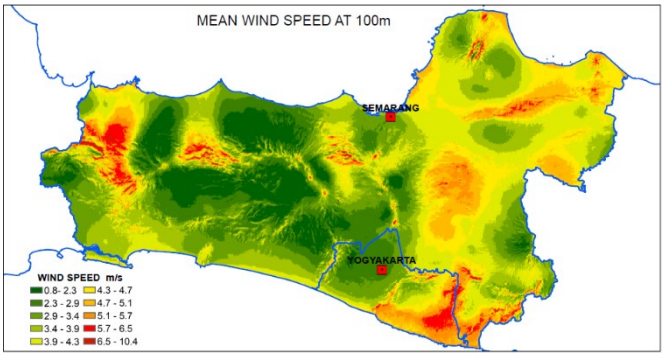


Fig. 4. Wind potential map of Gunung Kidul.

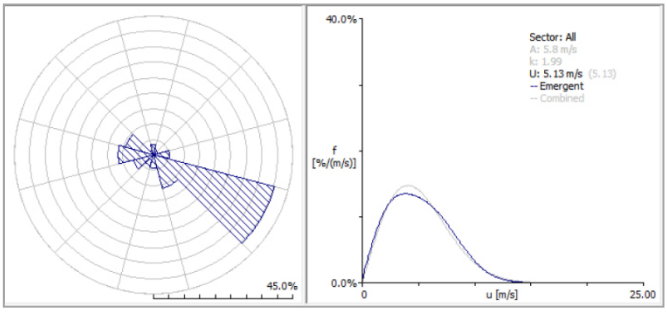


Fig. 5. Wind direction and speed distribution.

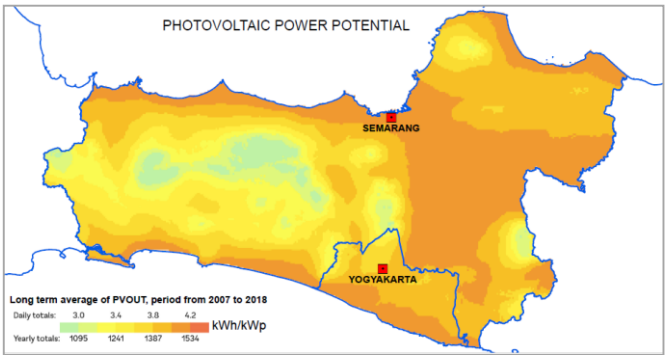


Fig. 6. Wind direction and speed distribution.

Table 1. Wind speed distribution (number of events).

Wind speed	Number of events		
m/s	50 meters	35 meters	20 meters
0-1	733	798	930
1-2	3.428	3.768	4.496
2-3	5.599	6.259	7.581
3-4	6.296	7.063	8.342
4-5	6.492	6.453	6.997
5-6	5.425	5.300	5.591
6-7	4.558	4.224	4.225
7-8	3.882	3.720	3.149
8-9	3.145	3.009	2.079
9-10	2.661	2.337	1.238
10-11	1.640	1.334	520
11-12	904	710	163
12-13	425	306	47
13-14	156	88	22
14-15	44	22	13
15-16	11	8	6
16-17	7	4	3
17-18	2	2	2
19-20	2	2	1
20-21	1	1	0
21-22	0	0	0
22-23	0	0	0
23-24	0	0	0
24-25	0	0	0

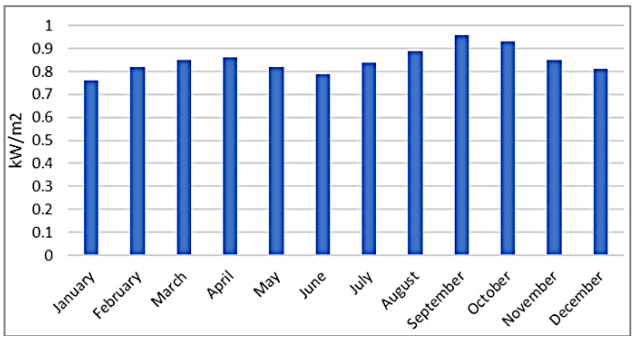


Fig 7. Solar radiation potential at Baron from Homer.

2.3. Floating LiDAR System (FLS)

The lack of a power grid offshore is an obstacle to supplying electricity for FLS loads, such as a LiDAR unit, sensors, data loggers, communication systems, navigation aids, and other accessories. The FLS power supplies may consist of photovoltaic (PV), wind turbine (WTG), backup power (fuel cell/FC or diesel generator/DEG) and battery to store the excess energy. It depends on the availability of renewable energy resources and economic considerations. Table 2 lists several commercial and pre-commercial FLS that use various renewable energy sources with diesel or fuel cells as a backup. FLS Fugro and FLS Fraunhofer's renewable capacity are smaller than other FLS, but they have backup power.

Table 2. List of Floating LiDAR System.

Floating LiDAR System			Energy
Name	Manufacturer	LiDAR	Supply
FLiDAR Windsentinel™	AXYS Technologies	Zephyr or Windcube	PV-WTG-DEG
SEAWATCH® Wind LiDAR Buoy	FUGRO	Zephyr	PV-FC
Fraunhofer IWES wind LiDAR buoy	Fraunhofer IWES	Zephyr or Windcube	PV-WTG-DEG-FC
EOLOS FLS200	EOLOS Floating LiDAR Solution	Zephyr	PV-WTG
ACCURASEA Floating LiDAR Buoy	BLIDAR consortium	Windcube	PV-WTG
DeepCLiDAR	AWS Truepower	Windcube	PV-WTG
RPS Floating LiDAR buoy	RPS	Zephyr	PV-WTG
Molas B300M	Nanjing Movelaser Technology	Molas	PV-WTG

Three technology providers of LiDAR are normally used on offshore platforms, i.e., the Zephyr Z300 from Campbell Scientific, the WindCube from Vaisala, and the Molas B300M from Nanjing Movelaser Technology, as shown in Table 3.

Table 3. Technical Specification of LiDAR.

Specification	Unit	Zephyr Z300	WindCube	Molas B300M
Temperature range	°C	-40°- +50	-30°- +50	-40°- +50
Power consumption	Watt	69	45	70
Weight	kg	55	59	<75
Measurement range	meter	10-200	40-300	40-300
Sampling rate	Hz	50	User define	1
Scanning cone angle	°	30	28	28
Wind speed range	m/s	<1 - 70	0 - 60	0 - 75
Wind speed accuracy	%	<0.5	0.1	0.1
Wind speed direction accuracy	°	<0.5	2	1
Wind speed direction accuracy	°	<0.5	2	1
Protection		IP67	IP67	IP67

2.4. The FLS Power Supplies

The FLS power supplies may consist of photovoltaic, wind turbine, backup power (fuel cell or diesel) and battery to store the excess energy. The concept of integrated power system operation is to supply energy from photovoltaic cells and wind turbines for load demand and battery charging, as illustrated in Fig 8. If renewable energy sources are insufficient for load demand, a difference of energy is provided from the battery or fuel cell backup if the battery is discharged.

2.4.1. Photovoltaic

Photovoltaic (PV) is a device that converts solar energy directly into electricity. The PV panel's output is strongly affected by the amount of solar radiation it receives. The PV module output power would reach nearly its rated power if the solar radiation received by the PV module is at STC condition (1,000 W/m^2). The cell temperature also affects power output, such that as the temperature increases, the power output decreases due to the characteristics of PV cells, which are represented as a PV temperature coefficient of pow. Homer defines the PV power output as follow

$$P_{PV} = P_{Nom} \times \frac{H_{T(t)}}{H_{T(STC)}} \times \left[1 + \propto_P \times \left(T_{C(t)} - T_{C(STC)}\right)\right] \quad (1)$$

$$E_{PV} = P_{Nom} \times Hr_{day} \quad (2)$$

where P_{PV} is the power output of the PV module in watts, P_{Nom} is the nominal power output PV module in Wp, $H_{T(t)}$ is solar radiation on the PV module at the current Time in W/m^2, $H_{T(STC)}$ is solar radiation on the PV module in STC equal to 1000 W/m^2, α_P is temperature coefficient of power in %/°C, $T_{C(t)}$ is PV cell temperature at the current Time in °C, $T_{C(STC)}$ is PV's cell temperature at STC in 25°C, E_{PV} is daily energy output in Wh/m^2, and Hr_{day} is a total hour during which the solar radiation is at a maximum in an hour.

2.4.2. Wind turbine

A wind turbine is a device that converts the kinetic energy of wind into electrical energy [20]. The theoretical wind power output from wind flowing through the swept area A of a rotor during time t is [21]:

$$P_{WTG} = \frac{1}{2} \times \rho \times A \times v^3 \quad (3)$$

where P_{WTG}, ρ, A, and v are the power output of the wind turbine in watts, air density in kg/m^3, wind turbine rotor swept area in m^2, and wind speed in m/s, respectively. However, wind speed has randomness, volatility, and intermittent characteristics, making the output power of a wind turbine fluctuate considerably. Therefore, the above formula can be reformulated into:

$$P = \int_0^\infty P_{WTG} \times f(v) \times dv \quad (4)$$

where $f(v)$ is the probability density function of wind speed.

The Weibull probability distribution has been widely used in wind analysis, planning, design, construction, and operation.

$$f(v) = \frac{k}{C} \times \left(\frac{v}{C}\right)^{k-1} \times e^{-\left(\frac{v}{C}\right)^k} \quad (5)$$

$$k > 0; U > 0; C > 1$$

The Weibull probability density function of observed wind speed v (m/s) is represented by $f(v)$, the Weibull scale parameter in m/s is defined by C, and the dimensionless Weibull shape parameter is represented by k [22]. The Weibull shape parameter k has values between 1 and 3 and describes wind behavior by its speed; where small values of k show variations in wind variables, a rather constant wind speed can be shown with a large k value [23, 24].

2.4.3. Backup power (Fuel Cell or Diesel)

A fuel cell (FC) is a device that converts the chemical energy of fuel (hydrogen) and an oxidant (air or oxygen) into electricity by electrochemical reaction with byproducts are water and heat [25]. Hydrogen can be produced with electricity via electrochemical process of water through the electrolyzer [26]. The FC supplies electricity if the load demands exceed the generated electricity from the integrated renewable system. When the integrated renewable system drops, FC can serve as an emergency generator [27]. A diesel generator, also known as a diesel genset, combines a diesel engine with an electric generator to generate electrical energy. Diesel genset is used in places without connection to a power grid or as an emergency power supply if the grid fails.

2.4.4. Battery

A battery storage device stores direct electrical energy in an electrochemical configuration for later use. The battery controller controls the capacity of energy that will be stored or delivered from the battery. The battery is used for storing when excessive energy is available and discharging when energy is required.

2.4.5. Optimization of the FLS power supplies

The operation concept of the hybrid power system is to supply renewable power (photovoltaics and wind turbines) to load demand and battery charging. If renewable energy sources are insufficient for energy demand, a difference of energy is provided from the battery or fuel cell backup if the battery is discharged. Figure 8 depicts the hybrid model (PV-wind-backup power) that simulates the FLS's optimization power supply. The total annual energy consumed by the FLS load should equal the total energy supply from solar PV and wind turbines. The diesel or fuel cell serves only as a backup power source if renewable energy fails to deliver power.

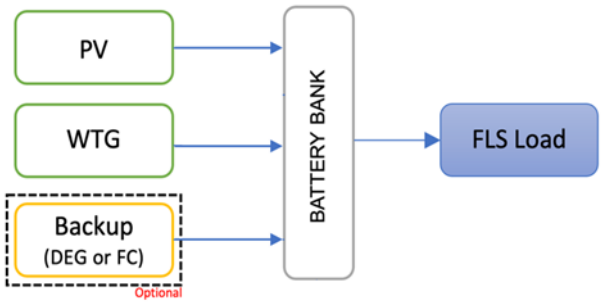


Fig 8. Model of hybrid PV-wind-backup power.

Even though the availability of solar and wind energy resources may be predicted based on historical data, it cannot be 100% guaranteed; therefore, the size of the energy load should be multiplied by the safety factor greater than 1, as shown in Equation 6.

If it is assumed there are no losses in the battery bank, then,

$$E_{SUPPLY} = E_{LOAD} \times safety\ factor \quad (6)$$

$$E_{SUPPLY} = E_{BAT} \quad (7)$$

$$E_{SUPPLY} = E_{PV} + E_{WTG} + E_{BU} \quad (8)$$

where E_{SUPPLY}, E_{LOAD}, and E_{BAT} are total annual energy provided by system, energy consumed by FLS load and energy stored by batteries, respectively. The safety factor is a number that indicates the amount of reserve power, which is generally stated to be more than one. E_{PV}, Ew_{TG}, and E_{BU} are the total annual energy from PV, WTG, and backup power respectively.

$$E_{PV} = N_{PV} \times P_{PV}(S) \times T_{PV} \quad (9)$$

$$E_{WTG} = N_{WTG} \times P_{WTG}(S) \times T_{WTG} \quad (10)$$

$$E_{BU} = N_{BU} \times P_{BU}(S) \times T_{BU} \quad (11)$$

P_{PV}, P_{WTG}, and P_{BU} are the capacity of the PV module, the capacity of WTG, and the capacity of backup power, respectively. N_{PV}, N_{WTG}, and N_{BU} are the unit number of the PV module, WTG, and backup power, respectively. In this study, the single capacities used for solar cells, wind turbines, and generators are 50-Watt peak, 400 Watt, and 500 Watt, respectively. T_{PV}, T_{WTG}, and T_{BU} are the operation time of the PV module, WTG, and backup power, respectively.

Energy optimization is carried out by defining objective functions, namely minimizing energy generation costs (*Min* $GC_{Esupply}$); installation costs (IC_{PV}, IC_{WT}, and IC_{BU}); replacement costs (RC_{PV}, RC_{WT}, and RC_{BU}); operation and maintenance costs (OC_{PV}, OC_{WT}, and OC_{BU}); and residual values (S_{PV}, S_{WT}, and S_{BU}) during the planning period. The PV, WT, and BU codes indicate the generation type of solar cells, wind turbines, and generators, respectively.

To obtain the optimum size of power supplies, it is necessary to optimize the process with the objective function of minimizing energy generating costs (GC). The objective function is given in Equation 12,

$$O_{bj} = Min\ GC_{E\ Supply} = (1 + r^n) \times \sum IC_X + G_{CX} + R_{CX} - S_X \quad (12)$$

where X is for each generation type of solar cells, wind turbines, and generators (PV, WT, and BU). In the generation planning system, the discount rate affects the cost factor, which is expressed in the equation $(1+r^n)$, where n is the planning period, and r is the value of the discount rate.

The limiting function of the objective above is the availability of area for the floating LiDAR system (FLS), and based on the data obtained, the effective area of LiDAR that can be used is 12 m^2. This equation can be expressed as the following:

$$A_{PV} + A_{WT} + A_{BU} \leq A_{FLS} \quad (13)$$

where A_{PV} is the area for installing solar cell modules, A_{WT} is the area for installing wind turbines, A_{BU} is the area for placing generators, and A_{FLS} is the area for installing FLS energy sources. In this study, based on the data obtained, the area per solar cell module is 0.5 m^2, and the wind turbine is 2 m^2, while the generator set is ignored because it can be placed inside the FLS system.

We calculate the optimization of generator configurations in various safety factors. If the safety factor in Eq. (8) is denoted as *SF*, then the constraint is shown in Eq. (14). Since the safety factors value is not the exact number and the single capacity of generators has been decided, we have the excess energy from the optimization result. The excess energy formula is defined as the energy supply of the optimization result minus energy requirements from the selected safety factor.

$$(1 - 0{,}03)SF_x \leq SF_x \leq (1 + 0{,}03)SF_x \quad (14)$$

2.4.6. Energy generating cost

Levelized Cost of Energy (LCOE) is the cost of generating energy for a particular system. It is an economic assessment of the cost of the energy-generating system, including all the costs over its lifetime: initial investment, operations and maintenance, cost of fuel, and cost of capital [28]. A net present value calculation is performed and solved so that for the value of the LCOE chosen, the project's net present value becomes zero [29]. This means that the LCOE is the minimum price at which energy must be sold for an energy project to break even. Typically, LCOEs are calculated over 20~40-year lifetimes and are given in the units of currency per kilowatt-hour, for example, USD/kWh or per megawatt-hour.

$$LCOE = \frac{Cost\ of\ System}{Energy\ Production} \quad (15)$$

$$LCOE = \frac{IC + OM + R - S}{EP} \quad (16)$$

IC is initial or capital cost, *OM* is operation and maintenance cost, *R* is replacement cost *S* is salvage value, and *EP* is energy production.

Figure 9 depicts the flow chart used in this study to determine the optimal value of the energy mix that can be used to deliver FLS power.

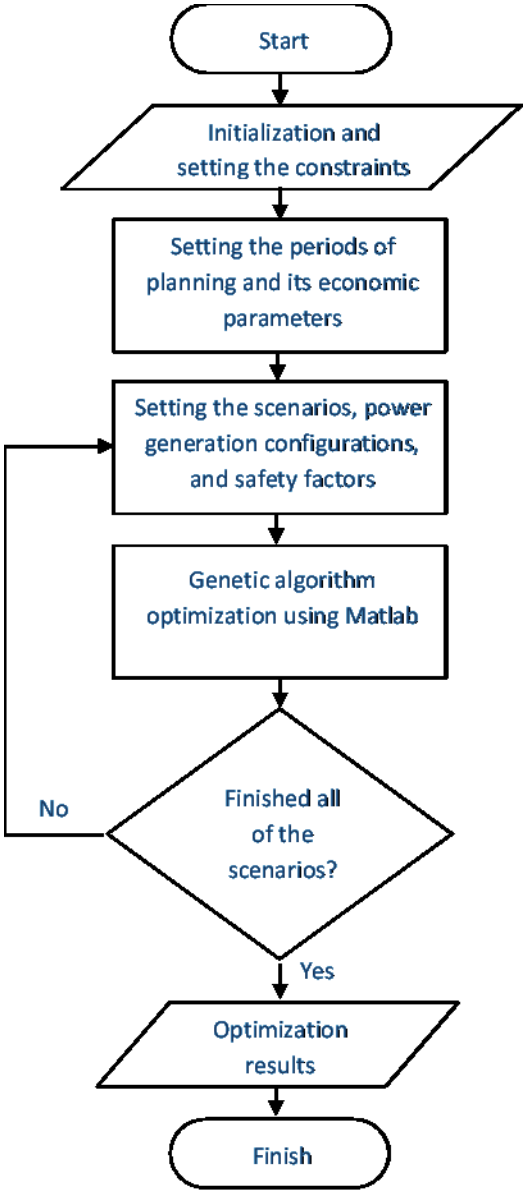


Fig.9. Flow chart of the study

3. Results and Discussions

3.1. The FLS Loads

From previous several commercial and pre-commercial FLS, it can be depicted in the block diagram of the FLS that consists of solar PV, wind turbine, battery and fuel cell or diesel as a backup power in Fig. 10. The daily energy consumption based on the assumption of load operations every day is shown in Table 4. The obstruction light (OB) will be operated during nighttime only. Meanwhile, the LiDAR

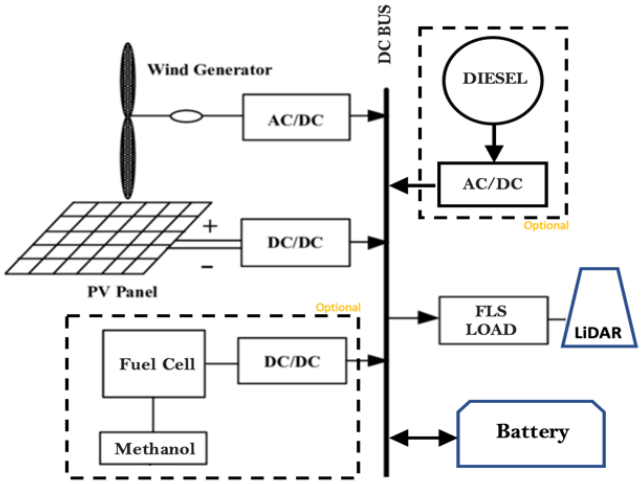


Fig. 10. Block diagram of the Floating LiDAR System

washer (water pump + wiper) will be operated intermittently only if the LiDAR glass cover is dirty (assumed to operate one minute every hour). The power consumption of WindCube LiDAR is the lowest (45W), then Zephyr Z300 (69W) and molas B300M (70W) is the biggest.

The daily load profile of the FLS, solar radiation and wind speed on the Baron Coast can be seen in Fig. 11.

Table 4. Daily energy consumption

FLS Load	Duration (hr)	Power (W)	Energy (Wh)
LiDAR	24	45 - 70	1,080 - 1,680
Obstruction Light	12	10	120
LiDAR Washer (water pump and wiper)	0.5	20	10
Data Logging	24	10	240
Data Communication	24	10	240
Daily Power or Energy Consumption		95 - 120	1,690 - 2,290

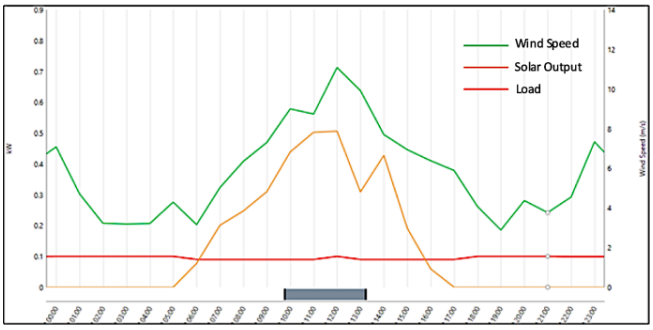


Fig. 11. Daily load profile of the FLS, solar radiation and wind speed.

3.2. Optimization of the FLS Power Supplies

Optimization of power generator selection is carried out using three scenarios. The first scenario is competition between types of generators, as shown in Table 5, with variations in safety factors. The second scenario includes a backup system as an energy source other than photovoltaic, with a variation of the safety factor. The third scenario is using wind turbines that are forced into the system.

In the first scenario, competition between types of power plants with variations in the factor of safety results is shown in Table 5. With various safety factors, the PV generators are superior, with a total energy supply cost per year per kWh of IDR 5,200. An increase in the safety factor indicates a larger kWh energy supply than needed and, at the same time, requires a larger area for PV placement. Based on the proposed design, the limited area of PV panels can provide a maximum safety factor of 2.2. This number of safety factors means the annual power supply is 1,838.87 kWh or 2.2 times the load needed. Using 24 solar panels of 50 Wp will produce more than 0.73 kWh of energy per year, assuming 2.2 times LiDAR energy requirements. In this scenario, a safety factor of 2.2 is the optimal choice, even though the installation costs is the highest, the LCOE is the same, and the excess energy is the lowest compared to other safety factor values.

In this case study, only installation costs are incurred for PV installation. The planning period is 24 years, during which there is no replacement of the PV generator, and the residual value of the PV panels is considered zero or worthless. Table 6 shows the total cost of generation from the Scenario 1 variation in the safety factor.

Considering the additional type of generators, in Scenario 2 and Scenario 3, we set the maximum safety factor as 2. In Scenario 2, we include a diesel generator as a backup in the generation system competition. It is a single capacity of 500 Watt, assuming the generation cost is shown in Table 7 and 12 years of lifetime. The results of the competition are shown in Table 7. In Scenario 2, the diesel generator as a backup is forced into the system and the operation scenarios are one and two hours a day. These operation scenarios produce the amount of energy per year are 182.5 kWh and 365 kWh, respectively. Using a backup system does not reduce the area of use of PV panels in floating LiDAR systems. In the condition of the safety factor is 2, using a diesel generator for one hour a day will reduce the capacity of PV from 1100 Wp in Scenario 1 to 1000 Wp in Scenario 2. Meanwhile, using a diesel generator for two hours a day will reduce the capacity of PV to 850 Wp, but as a consequence, more CO_2 emission is released.

In Scenario 2, increasing the number of diesel generator operating hours will increase the generation cost, especially the operational costs. A higher safety factor means a higher capacity of PV for the same diesel generator operating hour. The higher number of safety factors increases the total cost but not the LCOE. The LCOE for a safety factor 2 is lower than the safety factor 1.8 at the same diesel generator operating hours. The optimum cost for this scenario is configuration of 1000 Wp of PV with safety factor of 2 and an hour a day of diesel generator operating hours. However, the minimum excess energy is Case 5 with PV capacity of 750 kWp, safety factor of 1.8 and two hours a day of diesel generator. The cost of generations for various safety factors is shown in Table 8.

Table 5. Generators output with variation of safety factors in Scenario 1

Case	Safety Factor	Supply	PV		WTG		Backup		Excess
		kWh	Wp	kWh	W	kWh	W	kWh	kWh
1	1.4	1170.19	750	1150	0	0	0	0	-20.4
2	1.6	1337.36	850	1303	0	0	0	0	-34.3
3	1.8	1504.53	1000	1533	0	0	0	0	28.5
4	2	1671.70	1100	1686	0	0	0	0	14.6
5	2.1	1755.28	1150	1763	0	0	0	0	7.7
6	2.2	1838.87	1200	1840	0	0	0	0	0.73

Table 6. Generation costs with variation of safety factors in Scenario 1

Case	Safety Factor	Installation Cost (1.000 IDR)			Replacement Cost (1.000 IDR)			Operation Cost (1.000 IDR)			Salvage Value (1.000 IDR)			Total Cost (1.000 IDR)	
		PV	WT	BU	PV	WT	BU	PV	WT	BU	PV	WT	BU	All	/kWh
1	1,4	5.925	0	0			0			0			0	5.925	5,2
2	1,6	6.715	0	0										6.715	5,2
3	1,8	7.900	0	0										7.900	5,2
4	2	8.690	0	0										8.690	5,2
5	2,1	9.085	0	0										9.085	5,2
6	2,2	9.480	0	0										9.480	5,2

Table 7. Generator output with variation of safety factors in Scenario 2

Case	Safety Factor	Supply	PV		WTG		Backup		Excess
		kWh	Wp	kWh	W	kWh	W	kWh	kWh
1	1.6	1337.36	750	1150	0	0	500	182.5	-5.11
2	1.8	1504.53	850	1303	0	0	500	182.5	-18.98
3	2	1671.7	1000	1533	0	0	500	182.5	43.8
4	1.6	1337.36	650	996	0	0	500	365	24.09
5	1.8	1671.7	750	1150	0	0	500	365	10.22
6	2	1755.28	850	1303	0	0	500	365	-3.65

Table 8. Generation costs with variation of safety factors in Scenario 2

Case	Safety Factor	Installation Cost (1.000 IDR)			Replacement Cost (1.000 IDR)			Operation Cost (1.000 IDR)			Salvage Cost (1.000 IDR)			Total Cost (1.000 IDR)	
		PV	WT	BU	PV	WT	BU	PV	WT	BU	PV	WT	BU	All	/kWh
1	1.6	5,925	0	7,500	0	0	18,886	0	0	9,707	0	0	19,024	22,995	17.3
2	1.8	6,715	0	7,500	0	0	18,886	0	0	9,707	0	0	19,024	23,785	16.0
3	2	7,900	0	7,500	0	0	18,886	0	0	9,707	0	0	19,024	24,970	14.6
4	1.6	5,135	0	7,500	0	0	18,886	0	0	19,414	0	0	19,024	31.912	23.4
5	1.8	5,925	0	7,500	0	0	18,886	0	0	19,414	0	0	19,024	32,702	21.6
6	2	6,715	0	7,500	0	0	18,886	0	0	19,414	0	0	19,024	33,493	20.1

The last scenario is a competition between PV dan WTG without a backup system. A single WTG generated 400 W implemented in the system; the result is shown in Table 9. Based on the availability of the wind speed data, the availability factor of a single WTG in a year is 1,314 hours. If only considering the annual energy, WTGs are a potential power generator to be installed for replacing a backup system. Due to WTG need a 2 m^2 of area, the maximum PV installed is 20 panels of single 50 Wp of PV.

Table 10 shows the total cost of generation for Scenario 3 in various safety factors. If the initial cost of the WTG is higher than PV or a backup system, then it makes costly in comparison to the previous scenarios. The trend of the safety factor scenario for LCOE is the same, in which a higher safety factor will reduce the amount of LCOE. In scenario 3, we need to install 750 Wp to get the number of safety factors 2.

From Tables 6, 8 and 10, the costs obtained in Scenario 1 are relatively smaller when compared to the other scenarios. This is why PV is always superior when competing with other types of generators. Table 11 shows the selected configuration based on the optimum capacity of each generator and the minimum cost. The LCOE winners are Scenario 1, Scenario 2, and Scenario 3, respectively. It means 1.2 kW of PV on the platform can fulfill the energy demand of the floating LiDAR system. Another option is 750 Wp of PV with 500 W of backup system or 400 W of WTG generator. It needs a higher safety factor if only using a single type of generator, such as PV. The diesel generator as a backup technology is more reliable than a WTG. Then, the safety factor for a combination of PV and a backup system can be set to lower than a combination of PV and WTG.

Table 9. Generator output with variation of safety factors in Scenario 3.

Case	Safety Factor	Supply	PV		WTG		Backup		Excess
		kWh	Wp	kWh	W	kWh	W	kWh	kWh
1	1.4	1170.19	400	613	400	525.6	0	0	-31.39
2	1.6	1337.36	550	843	400	525.6	0	0	31.39
3	1.8	1504.53	650	996	400	525.6	0	0	17.52
4	2	1671.7	750	1150	400	525.6	0	0	3.65

Table 10. Generation costs with variation of safety factors in Scenario 3.

Case	Safety Factor	Installation Cost (1.000 IDR)			Replacement Cost (1.000 IDR)			Operation Cost (1.000 IDR)			Salvage Cost (1.000 IDR)			Total Cost (1.000 IDR)	
		PV	WT	BU	PV	WT	BU	PV	WT	BU	PV	WT	BU	All	/kWh
1	1.4	3,160	15,000	0	0	37,773	0	0	29,160	0	0	19,024	0	66,069	58.0
2	1.6	4,345	15,000	0	0	37,773	0	0	29,160	0	0	19,024	0	67,254	49.1
3	1.8	5,135	15,000	0	0	37,773	0	0	29,160	0	0	19,024	0	68,044	44.7
4	2	5,925	15,000	0	0	37,773	0	1	29,160	0	0	19,024	0	68,835	41.1

Table 11. Generator output with variation of safety factors for three scenarios.

Scenario	Safety Factor	Supply	PV		WTG		Backup		Excess	LCOE (1.000 IDR/kWh)
		kWh	Wp	kWh	W	kWh	W	kWh	kWh	
1	2.2	1838.9	1200	1840	0	0	0	0	0.7	5.2
2	1.8	1671.7	750	1150	0	0	500	365	10.22	21.6
3	2	1671.7	750	1150	400	525.6	0	0	3.65	41.1

3.3. Homer Analysis of Hybrid System (PV-Wind-Backup Power)

Figure 12 shows the block diagram of the PV/Wind Hybrid system in Homer simulation. The maximum daily energy load is about 2,29 kWh/day. The simulation results offer four cases with different combination of generator and its capacity as shown in Tabel 12. The FLS's battery capacity is fixed at 4,92 kWh. Cases 1 – 3 are the same power generation combination as in the simulation scenarios using GA. From the results in Tables 12 and 13, it can be inferred that the lowest energy generation cost is Case 1, with a PV capacity of 1200 Wp, followed by Case 2 and Case 3. These results validate the GA-based simulation results that 100% PV is the optimum solution for powering the FLS load.

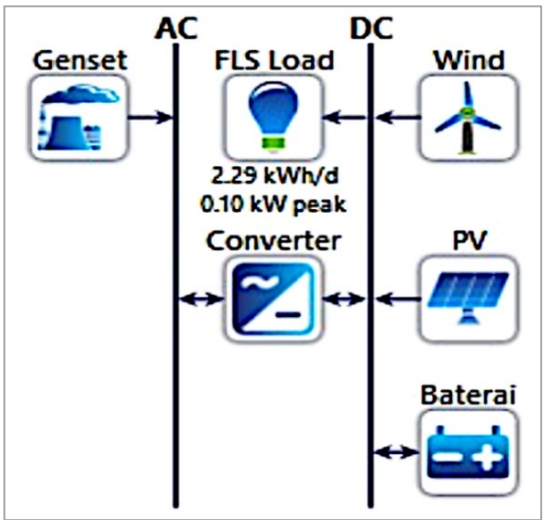


Fig. 12. Hybrid power supplies of FLS in Homer simulation.

Table 12. Generetors output optimization result.

Case	PV (Wp)	WTG (W)	Backup DG (W)	LCOE (IDR/kWh)
1	1200	-	-	3608
2	700	-	500	3629
3	1000	400	-	6783
4	700	400	500	6980

Table 13. Optimization result of the generated energy.

Case	PV		WTG		Backup		Supply	Excess
	kWh	%	kWh	%	kWh	%	kWh	kWh
1	2006	100	-	-	-	-	2006	1085
2	1170	99.1	-	-	11.1	0.942	1181	259
3	1672	97.7	39.6	2.32	-	-	1711	792
4	1170	95.9	39.6	3.25	10.4	0.85	1220	301

4. Conclusion

This paper presents the optimization of energy supplies for the Floating LiDAR System at Baron Coast with various scenarios using the genetic algorithm method and Homer simulation. The three candidates for power generator and the three scenarios, including various safety factors, are implemented. In the scenario of competition only considering LCOE for Scenario 1, the PV is dominant and considering the FLS area, the maximum safety factor is 2.2. Scenario 2 was chosen in the condition that set the backup into the system; the safety factor is 1.8. To force WTs into the system for making various renewable energy in Scenario 3, the safety factor is 2 was considered. In general, more safety factors are less of LCOE for the same power generation configuration; meanwhile, there are some constraints, such as the FLS area, the initial cost, unmet load and the excess energy. A PV has less availability factor than others, followed by a WT and a

backup system. Therefore, the safety factors for only PV, PV and the backup, and PV and WT are 2.2, 1.8 and 2, respectively. Considering LCOE, both GA and Homer reveal that PV is the best candidate for powering the FLS. Meanwhile, the combination of PV and wind turbine shows the highest cost of energy solution for FLS supply.

In terms of installed capacity for Scenario 1 is 1,200 Wp of PV in both Homer and GA. Scenario 2 shows 750 Wp of PV and 500 W of backup system in GA; meanwhile, in Homer result is almost the same, where 700 of PV and 500 W of the backup system. Optimization of the Genetic Algorithm in Scenario 3 shows 750 Wp of PV and 400 W of WT, and a slightly different is shown in Homer, where 1000 Wp of PV and 400 W of WT.

References

[1] R. Wiser, M. Bolinger, B. Hoen, D. Millstein, J. Rand, G. Barbose, N. Darghouth, W. Gorman, S. Jeong, and B. Paulos, Land-based wind market report: 2022 edition, U.S. Department of Energy (DOE), 2022.

[2] S. Shimada, J. P. Goit, T. Ohsawa, T. Kogaki, and S. Nakamura, "Coastal wind measurements using a single scanning LiDAR," Remote Sens., vol. 12, no. 8, 2020.

[3] I. F. A. Vis and E. Ursavas, "Assessment approaches to logistics for offshore wind energy installation," Sustain. Energy Technol. Assessments, vol. 14, pp. 80–91, 2016.

[4] G. H. Ryu, Y. G. Kim, S. J. Kwak, M. S. Choi, M. S. Jeong, and C. J. Moon, "Atmospheric stability effects on offshore and coastal wind resource characteristics in South Korea for developing offshore wind farms," Energies, vol. 15, no. 4, 2022.

[5] C. B. Hasager and M. Sjöholm, Remote sensing of Atmospheric Conditions for Wind Energy Applications, MDPI, 2019.

[6] J. P. Goit, S. Shimada, and T. Kogaki, "Can Lidars replace meteorological masts in wind energy?," Energies, vol. 12, no. 19, pp. 1–24, 2019.

[7] O. Bischoff, I. Würth, J. Gottschall, B. Gribben, J. Hughes, D. Stein, H. Verhoef, Recommended Practices for Floating LiDAR System, The Carbon Trust, 2016.

[8] B. Akyol, M. D. Yazar, and E. Bekiroglu, "Technical feasibility of offshore wind power plant for Gökçeada Region in Türkiye," 12th IEEE Int. Conf. Renew. Energy Res. Appl. ICRERA 2023, pp. 517–523, 2023.

[9] J. Li and X. (Bill) Yu, "LiDAR technology for wind energy potential assessment: Demonstration and validation at a site around Lake Erie," Energy Convers. Manag., vol. 144, pp. 252–261, 2017.

[10] J. Gottschall, G. Wolken-Möhlmann, T. Viergutz, and B. Lange, "Results and conclusions of a floating-lidar offshore test," Energy Procedia, vol. 53, no. C, pp. 156–161, 2014.

[11] A. Viselli, M. Filippelli, N. Pettigrew, H. Dagher, and N. Faessler, "Validation of the first LiDAR wind resource assessment buoy system offshore the Northeast United States," Wind Energy, vol. 22, no. 11, pp. 1548–1562, 2019.

[12] A. Viselli, N. Faessler, and M. Filippelli, "LiDAR measurements of wind shear exponents and turbulence ıntensity offshore the Northeast United States," J. Offshore Mech. Arct. Eng., vol. 144, no. 4, pp. 1–9, 2022.

[13] A. Gautam, V. Warudkar, and J. L. Bhagoria, "Comparison of Weibull parameter estimation methods using LiDAR and mast wind data in an Indian offshore site: The Gulf of Khambhat," Ocean Eng., vol. 266, no. January, 2022.

[14] IEA, Floating Lidar Systems - Expert Group Report on Recommended Practices, International Energy Agency, 2017.

[15] H. Yang, W. Zhou, L. Lu, and Z. Fang, "Optimal sizing method for stand-alone hybrid solar-wind system with LPSP technology by using genetic algorithm," Sol. Energy, vol. 82, no. 4, pp. 354–367, 2008.

[16] G. P. Rajappa, "Solving Combinatorial Optimization Problems Using Genetic Algorithms and Ant Colony Optimization," University of Tennessee, 2012.

[17] Y. Astriani, K. Fauziah, H. Hilal, Riza, and B. Prasetyo, "Load sharing control between PV power plant and diesel generator to mitigate effect of PV fluctuation using PID algorithm," 2017 International Conference on High Voltage Engineering and Power Systems (ICHVEPS), Bali, pp. 140–144, 2-5 Oct. 2017.

[18] A. Oymak and M. R. Tür, "A short review on the optimization methods using for distributed generation planning," Int. J. Smart grid, vol. 6, no. V6i3, pp. 54–64, 2023.

[19] J. McMorland, M. Collu, D. McMillan, and J. Carroll, "Operation and maintenance for floating wind turbines: A review," Renew. Sustain. Energy Rev., vol. 163, p. 112499, 2022.

[20] O. Alkul, D. Syed, and S. Demirbas, "A review of wind energy conversion systems," 10th Int. Conf. Smart Grid, icSmartGrid 2022, pp. 72–77, 2022.

[21] I. Ifanda, D. Rostyono, R.P. Wijayanto, N. W. Hesty, A. Aziz, K. Fauziah, T. Zaky, A. Witjakso, A. Fudholi, "Optimizing turbine siting and wind farm layout in Indonesia," Int. J. Renew. Energy Res., vol. 13, no. 3, pp. 1351–1363, 2023.

[22] E. Rodrigo and A. Larico, "Wind energy potential by the weibull distribution at high-altitude peruvian highlands," Int. J. Smart grid, vol. 5, no. 3, 2021.

[23] F. H. Mahmood, A. K. Resen, and A. B. Khamees, "Wind characteristic analysis based on Weibull distribution of Al-Salman site, Iraq," Energy Reports, vol. 6, pp. 79–87, 2020.

[24] F. Azlan, J. C. Kurnia, B. T. Tan, and M. Z. Ismadi, "Review on optimisation methods of wind farm array

under three classical wind condition problems," Renew. Sustain. Energy Rev., vol. 135, August 2020.

[25] K. Fauziah et al., "Performance test of 1 kW PEM fuel cell system to determine ıts empirical model," Evergreen, vol. 10, no. 3, pp. 1982–1990, 2023.

[26] V. A. Martinez Lopez, H. Ziar, J. W. Haverkort, M. Zeman, and O. Isabella, "Dynamic operation of water electrolyzers: A review for applications in photovoltaic systems integration," Renew. Sustain. Energy Rev., vol. 182, p. 113407, May 2023.

[27] V. A. Ani, "Development of an Intelligent Power Management System for Solar PV-Wind-Battery-Fuel-Cell Integrated System," Front. Energy Res., vol. 9, pp. 1–14, March 2021.

[28] A. Monterrat, C. Carrejo, S. Hilliard, and F. Devaux, "Integration cost of variable renewable resources to power systems - a techno-economic assessment in european countries," 10th IEEE Int. Conf. Renew. Energy Res. Appl. ICRERA 2021, pp. 210–215, 2021.

[29] W. Short, D. Packey, and T. Holt, A Manual for the Economic Evaluation of Energy Efficiency and Renewable Energy Technologies, National Renewable Energy Lab. (NREL), 1995.